Electronic Supplementary Material (ESI) for ChemComm.

Electronic Supplementary Information

A Triad Molecular Conductor: Simultaneous Control of Charge and Molecular Arrangements

Naoya Kinoshita,[a] Atsuya Maruyama,[a] Takashi Shirahata,*[a,b] Toshio Naito,[b,c] and Yohji Misaki*[a,b]

[a] *Department of Applied Chemistry, Graduate School of Science and Engineering, Ehime University, Matsuyama 790-8577, Japan.*

[b] *Research Unit for Materials Development for Efficient Utilization and Storage of Energy, Ehime University, Matsuyama 790-8577, Japan.*

[c] *Department of Chemistry, Graduate School of Science and Engineering, Ehime University, Matsuyama 790-8577, Japan.*

Table of Contents

1.	General information	S2
2.	Experimental procedures and compounds characterization data	S2
3.	Preparation of single crystals of (**1**)PF_6	S3
4.	Cyclic voltammogram of the triad (**1**)	S4
5.	Measurement of the electrical resistivity	S4
6.	X-ray crystal structure analysis	S5
7.	Theoretical calculations	S12
8.	Band calculations	S13
9.	NMR spectra data	S17

1. General information

Unless otherwise noted, all reactions were performed under an argon atmosphere, and all reagents were purchased from commercial suppliers and used without further purification. ^{1}H NMR spectra were recorded on a Bruker Biospin AVANCE spectrometer using CS_2/C_6D_6 solvent at the Division of Applied Protein Research (APR), Ehime University. The chemical shifts were referenced to tetramethylsilane. MS spectra were determined on JEOL JMS-S3000. Melting points were determined with a Yanaco MP-500D. Cyclic voltammetry (CV) was carried out using an ALS/chi 617B electrochemical analyser. The CV cell consisted of a Pt working electrode, a Pt wire counter electrode, and an $Ag/AgNO_3$ reference electrode. The measurements were carried out in benzonitrile with a concentrate 0.1 M ^{n}Bu$_4$N$^+$PF$_6^-$ as a supporting electrolyte with a scan rate of 50 mV/s at 25 °C. All redox potentials were measured against Ag/Ag^+ and converted to *vs.* Fc/Fc^+.

2. Experimental procedures and compounds characterisation data

Synthesis of **3**

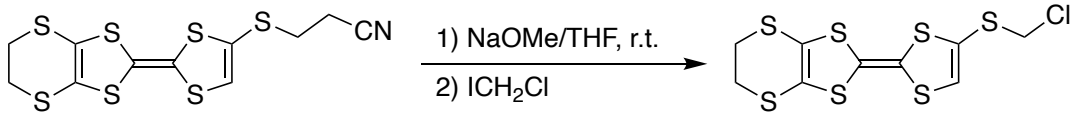

2 **3** (96%)

A solution of NaOMe (126 mg, 0.632 mmol) in MeOH was added dropwise to a solution of **2**[S1] (198 mg, 0.527 mmol) in THF (20 ml) at room temperature. The resultant mixture was stirred for 30 min at room temperature. Then, chloroiodomethane (58 µl, 0.79 mmol) was added dropwise. The reaction mixture was further stirred at room temperature for 1 h. The solvent was evaporated under reduced pressure. The residue was purified by column chromatography on silica gel with CH_2Cl_2 as the eluent, affording a yellow powder of **3** (190 mg, 0.507 mmol, 96%). m.p. 87–88 °C; ^{1}H NMR (400 MHz, CS_2/C_6D_6, 25 °C, TMS): 3.10 (s, 4H), 4.55 (s, 2H), 6.39 (s, 1H) ppm; ^{13}C NMR spectrum could not be obtained due to low solubility of **3** in a common solvent for NMR measurement.; IR (KBr): ν = 3065, 2990, 2917, 1549, 1502, 1421, 1396, 1290, 1230, 1145, 999, 929, 902, 858, 804, 779, 769, 712, 666, 631 cm^{-1}; HRMS (MALDI-TOF): *m*/*z* calcd. for $C_9H_7ClS_7$: 373.8281; found: 373.8274.

Synthesis of **4**

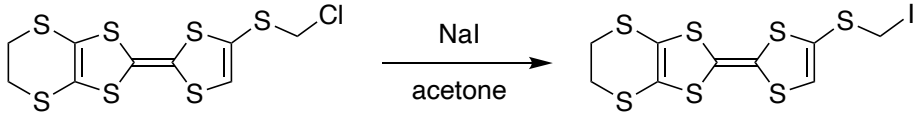

3 **4** (96%)

A mixed solution of NaI (198 mg, 1.32 mmol) and **3** (150 mg, 0.402 mmol) in acetone (15 ml) was refluxed for 4 h. After cooling to room temperature; the solvent was evaporated under reduced pressure. The residue was purified by column chromatography on silica gel with CH_2Cl_2 as the eluent, affording a yellow powder of **4** (187 mg, 0.386 mmol, 96%). m.p. 93–94 °C (decomp.); ^{1}H NMR (400 MHz, CS_2/C_6D_6, 25 °C, TMS): 3.11 (s, 4H), 4.24 (s, 2H), 6.37 (s, 1H) ppm; ^{13}C NMR spectrum could not be obtained due to low solubility of **4** in a common solvent for NMR measurement.; IR (KBr): 3065, 3005, 1425, 1284, 1138, 935, 900, 840, 807, 770, 692, 631 cm^{-1}; HRMS (MALDI-TOF): *m*/*z* calcd. for $C_9H_7IS_7$: 465.7637; found: 465.7630.

Synthesis of the triad (**1**)

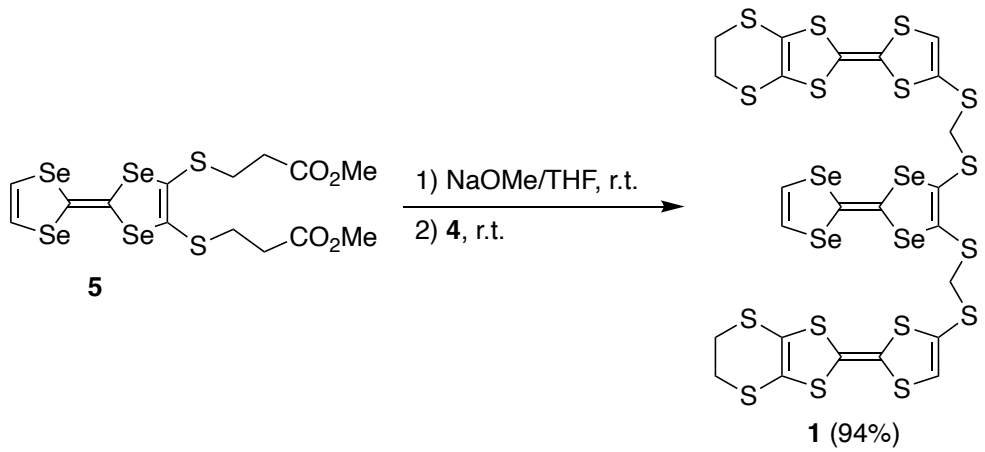

5

1 (94%)

A 28 wt% solution of NaOMe in MeOH (19 mg, 0.10 mmol) was added dropwise to a solution of **5**[S2] (30 mg, 0.048 mmol) in THF (5 ml) at room temperature. The resultant mixture was stirred for 30 min at room temperature after which **4** (47 mg, 0.10 mmol) was added. The reaction mixture was then stirred at room temperature for 1 h. The solvent was evaporated under reduced pressure; the residue was purified by column chromatography on silica gel with CS_2 as the eluent, affording an orange powder of **1** (51 mg, 0.045 mmol, 94%). m.p. 87–89 °C; ^{1}H NMR (400 MHz, CS_2/C_6D_6, 25 °C, TMS): 3.10 (s, 8H), 3.98 (s, 4H), 6.44 (s, 2H), 7.05 ppm (s, 2H); ^{13}C NMR spectrum could not be obtained owing to low solubility of **1** in a common solvent for NMR measurement.; IR (KBr): 3066, 2912, 1541, 1406, 1284, 1189, 931, 805, 770, 716, 667, 626 cm^{-1}; Elemental analysis: Calcd. (%) for $C_{24}H_{16}S_{16}Se_4$: C 25.44, H 1.42, found: C 25.37, H 1.59.

3. Preparation of single crystals of (**1**)PF_6

Single crystals of (**1**)PF_6 were prepared by electrochemical oxidation of a 1,2-dichloroethane (containing 6% ethanol, v/v, 18 ml) solution containing triad (**1**) (2.0 mg) and tetra-*n*-butylammonium (TBA) salts with PF_6 (28 mg) anions as the supporting electrolyte. Platinum wire electrodes (2.0 mm φ) and standard H-shaped cells were employed, and the applied current was changed stepwise from 0.2 to 0.5 μA at 25 °C for 7 days. Black elongated plates of (**1**)PF_6 were obtained.

4. Cyclic voltammogram of the triad (**1**)

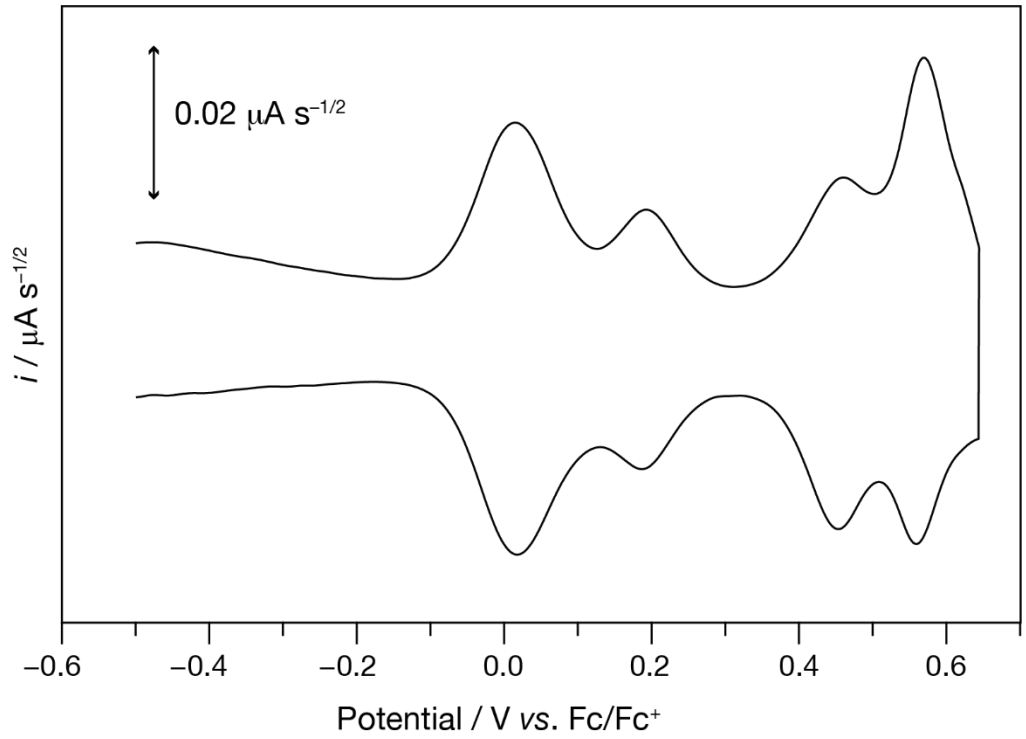

Figure S1. Deconvoluted cyclic voltammogram of the triad (**1**) in PhCN containing 0.1 M $^{n}Bu_4N^+PF_6^-$ at 25 °C using Pt working and counter electrodes. All potentials (V) were measured *vs*. Ag/Ag^+ and converted to the values *vs*. Fc/Fc^+.

5. Measurement of the electrical resistivity

The electrical resistivities were measured by a four-probe technique using direct current (100 μA). Gold wires (10 μm φ diameter) were attached to the single crystals using carbon paste. The samples were cooled down to around 58 K using a CryoMini cryostat (ULVAC CRYOGENICS INC, CRT-HE05-RE). The temperature was controlled using a Lakeshore S331 digital program temperature controller.

6. X-ray crystal structure analysis

The diffraction data of (**1**)PF_6 was collected using a Rigaku XtaLAB PRO diffractometer and multi-layer-mirror-monochromated Mo-Kα radiation. Raw frame data were integrated using CrysAlisPro,[S3] and the data were corrected by analytical absorption correction using a multifaceted crystal model based on expressions derived by R.C. Clark & J.S. Reid.[S4] The crystal structures were solved by the dual-space method (SHELXT-2018/2)[S5] and refined by full-matrix least-squares on F^2 (SHELXL-2019/3).[S6] Crystallographic data for (**1**)PF_6 are summarized in Table S1.

X-ray diffraction measurements at 50 and 100 K were conducted to obtain the structural information of Phase 2 and the intermediate phase. The lowering symmetry from *C*-lattice to *P*-lattice was suggested during the phase transition, and the CrysAlisPro and SHELXT utilities implied the space group $P2/c$ for the intermediate phase (100 K) and the space group $P2_1/n$ for Phase 2 (50 K). However, the refinement for these space groups did not converge.

Table S1. Crystallographic data of (**1**)PF_6 at 296, 120, 100, and 50 K.

	(**1**)PF_6			
formula	$C_{24}H_{16}F_6PS_{16}Se_4$			
T / K	296	120	100	50
crystal system	monoclinic	monoclinic	monoclinic	monoclinic
space group	*C*2/*c* (#15)	*C*2/*c* (#15)	*C*2/*c* (#15)	*C*2/*c* (#15)
a / Å	11.3183(6)	11.2588(3)	11.2465(5)	11.1972(4)
b / Å	28.7569(10)	28.5988(6)	28.5788(11)	28.5490(10)
c / Å	12.7846(6)	12.6211(3)	12.6059(6)	12.5806(6)
α / °	90	90	90	90
β / °	109.119(5)	109.992(3)	110.051(5)	110.047(4)
γ / °	90	90	90	90
V / Å^3	3931.6(3)	3818.96(17)	3806.1(3)	3778.0(3)
Z	4	4	4	4
D_{calc} / g cm^{-3}	2.159	2.223	2.231	2.247
μ / mm^{-1}	4.676	4.814	4.830	4.866
independent reflections	4506	4379	4362	4326
observed reflections [$I>2\sigma(I)$]	3299	3923	3740	3651
variable parameters	233	233	233	233
R_{int}	0.0205	0.0501	0.0218	0.0367
GOF	1.027	1.028	1.122	1.089
$R1$ [$I>2\sigma(I)$]	0.0448	0.0348	0.0475	0.0459
$wR2$ [$I>2\sigma(I)$]	0.0994	0.0904	0.0892	0.0979
$R1$ (all data)	0.0672	0.0400	0.0610	0.0587
$wR2$ (all data)	0.1075	0.0931	0.0934	0.1028
CCDC No.	2262519	2262520	2299528	2262521

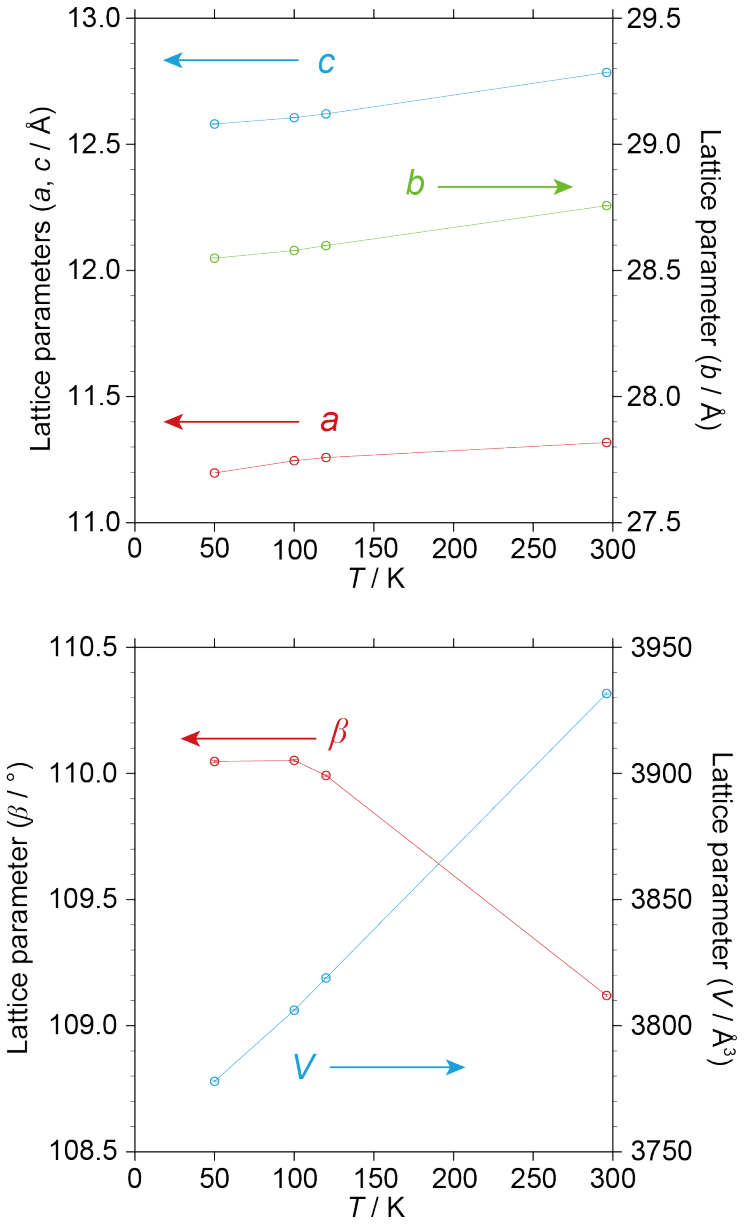

Figure S2. Lattice parameters of (**1**)PF_6 at (a) 296, (b) 120, (c) 100, and (d) 50 K.

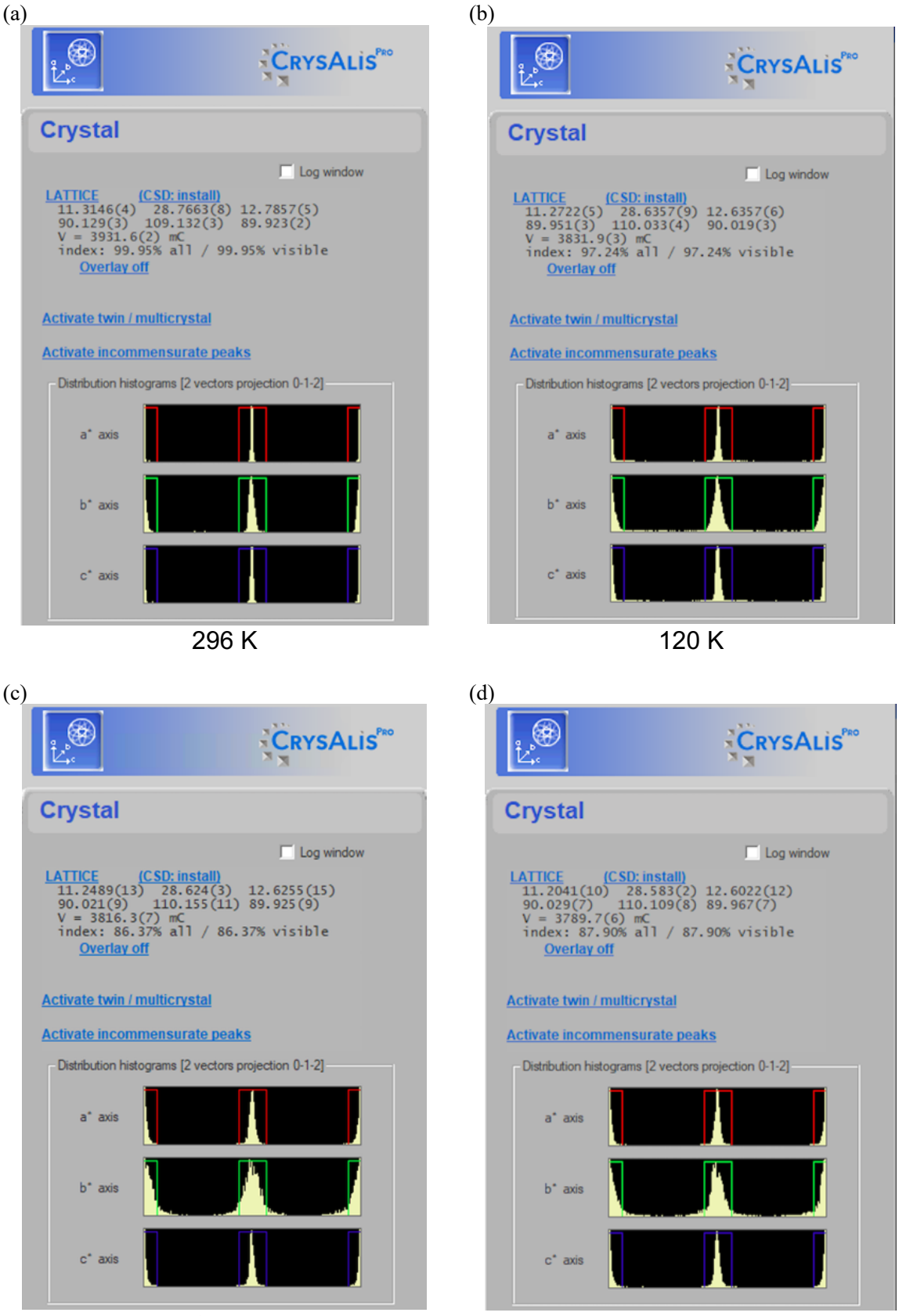

Figure S3. Distribution histograms of the *a**, *b**, and *c** axes obtained by the Ewald Explorer utility of CrysAlisPro[S3] at (a) 296, (b) 120, (c) 100, and (d) 50 K. Distribution histograms of *a**, *b**, and *c** axes at 296 and 120 K show a symmetrical shape. On the contrary, the split of the distribution histograms was shown in the *b** axis at 100 and 50 K.

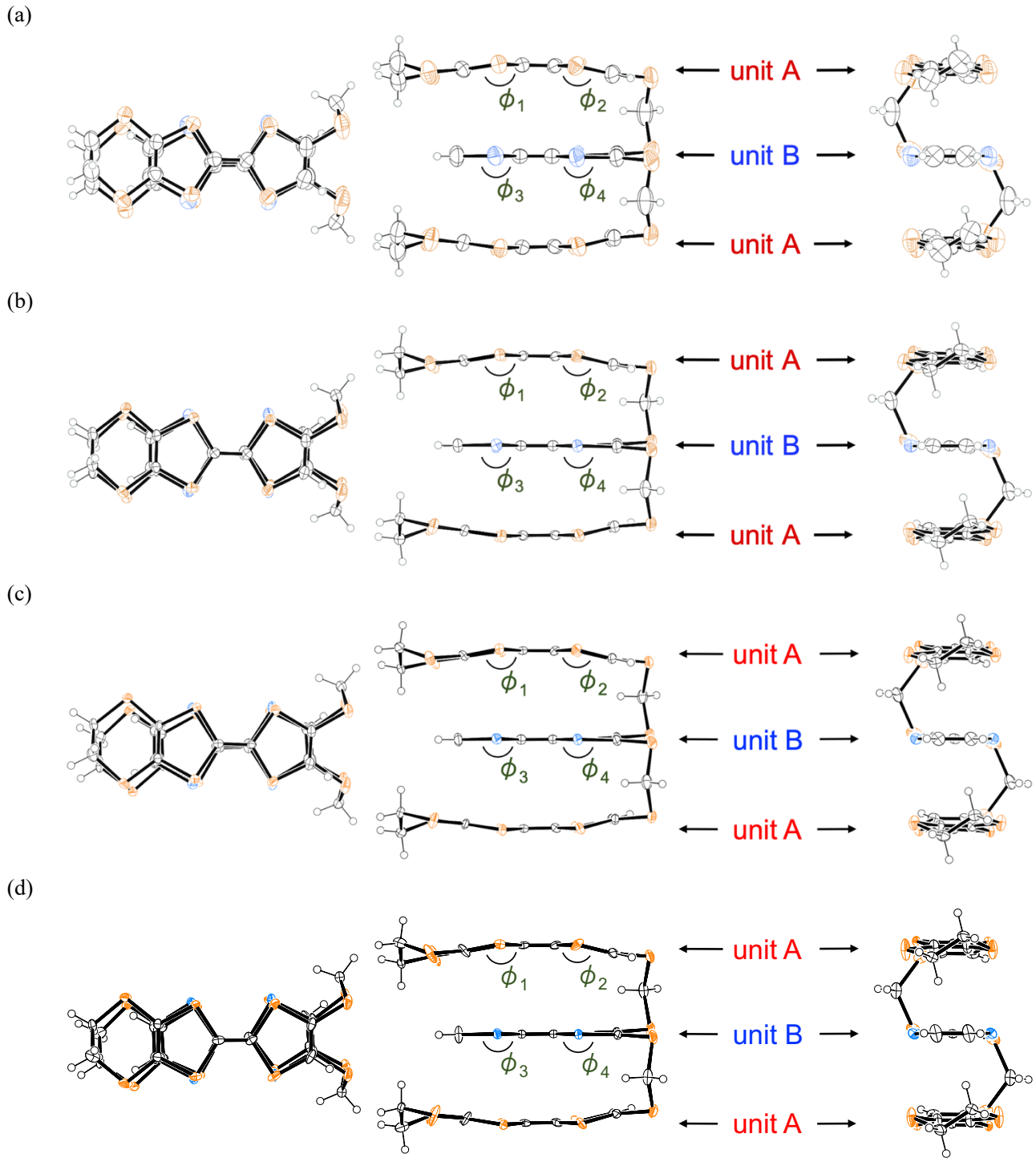

Figure S4. Molecular structures (top, side and end views) of the triad (**1**) in (**1**)PF_6 at (a) 296, (b) 120, (c) 100, and (d) 50 K. Folding angles ϕ_1, ϕ_2, ϕ_3, and ϕ_4 are listed in Table S2.

Table S2. Folding angles[a)] ϕ_1, ϕ_2, ϕ_3, and ϕ_4 of the triad (**1**) in (**1**)PF_6 at 296, 120, 100, and 50 K.

T / K	296	120	100	50
ϕ_1 / °	169.9	169.2	169.2	169.1
ϕ_2 / °	167.0	166.4	166.3	166.3
ϕ_3 / °	178.9	178.6	179.9	179.9
ϕ_4 / °	172.9	173.0	179.9	179.9

a) See Figure S4.

Table S3. Selected bond lengths of the donor molecule in (**1**)PF_6.

T / K		296	120	100	50
a / Å	C9–C10	1.354(5)	1.362(4)	1.357(5)	1.351(6)
b / Å	C7–C8	1.344(5)	1.343(4)	1.350(5)	1.350(6)
c / Å	C11–C12	1.324(6)	1.339(4)	1.334(6)	1.326(6)
d / Å	S4–C8	1.738(4)	1.748(3)	1.745(4)	1.741(4)
e / Å	S3–C7	1.742(3)	1.751(2)	1.746(4)	1.744(4)
f / Å	S4–C9	1.741(3)	1.741(2)	1.743(4)	1.743(4)
g / Å	S3–C9	1.736(3)	1.738(2)	1.739(4)	1.741(4)
h / Å	S6–C10	1.745(3)	1.743(2)	1.741(4)	1.742(4)
i / Å	S5–C10	1.738(4)	1.740(3)	1.745(4)	1.743(4)
j / Å	S6–C12	1.717(4)	1.724(3)	1.720(4)	1.721(4)
k / Å	S5–C11	1.763(4)	1.761(3)	1.764(4)	1.763(4)
a′ / Å	C2–C3	1.337(7)	1.343(6)	1.339(8)	1.341(8)
b′ / Å	C1–C1*	1.320(8)	1.328(6)	1.326(8)	1.321(9)
c′ / Å	C4–C4*	1.357(9)	1.349(7)	1.350(9)	1.343(9)
d′ / Å	Se1–C1	1.858(4)	1.872(3)	1.868(4)	1.869(4)
e′ / Å	Se1*–C1*	1.858(4) (= *d*′)	1.872(3) (= *d*′)	1.868(4) (= *d*′)	1.869(4) (= *d*′)
f′ / Å	Se1–C2	1.885(3)	1.888(2)	1.892(3)	1.887(3)
g′ / Å	Se1*–C2*	1.885(3) (= *f*′)	1.888(2) (= *f*′)	1.892(3) (= *f*′)	1.887(3) (= *f*′)
h′ / Å	Se2–C3	1.886(3)	1.886(2)	1.884(3)	1.885(3)
i′ / Å	Se2*–C3*	1.886(3) (= *h*′)	1.886(2) (= *h*′)	1.884(3) (= *h*′)	1.885(3) (= *h*′)
j′ / Å	Se2–C4	1.888(4)	1.896(3)	1.891(4)	1.895(4)
k′ / Å	Se2*–C4*	1.888(4) (= *j*′)	1.896(3) (= *j*′)	1.891(4) (= *j*′)	1.895(4) (= *j*′)

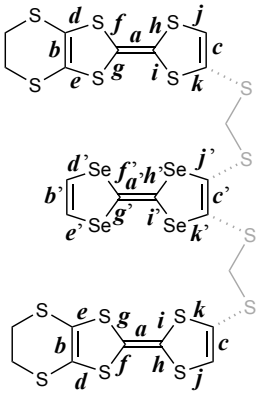

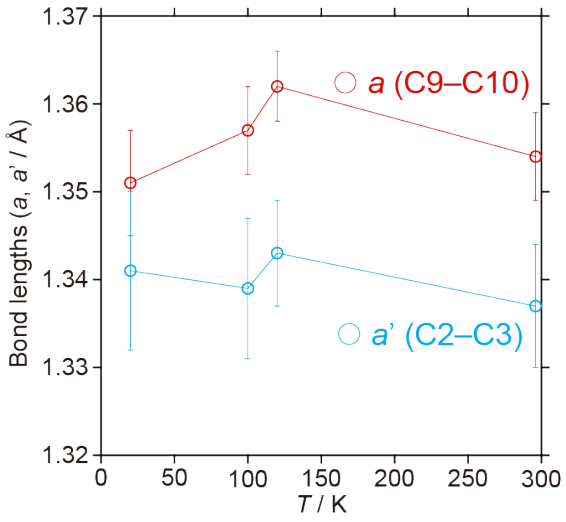

Figure S5. Bond lengths of *a* (C9–C10) and *a*' (C2–C3) of (**1**)PF_6 at (a) 296, (b) 120, (c) 100, and (d) 50 K.

*a*1 (Unit A–Unit B)

*a*2 (Unit A–Unit A)

Figure S6. Overlap modes of donor units *a*1 and *a*2 (top and side views) in (**1**)PF_6 at 296 K.

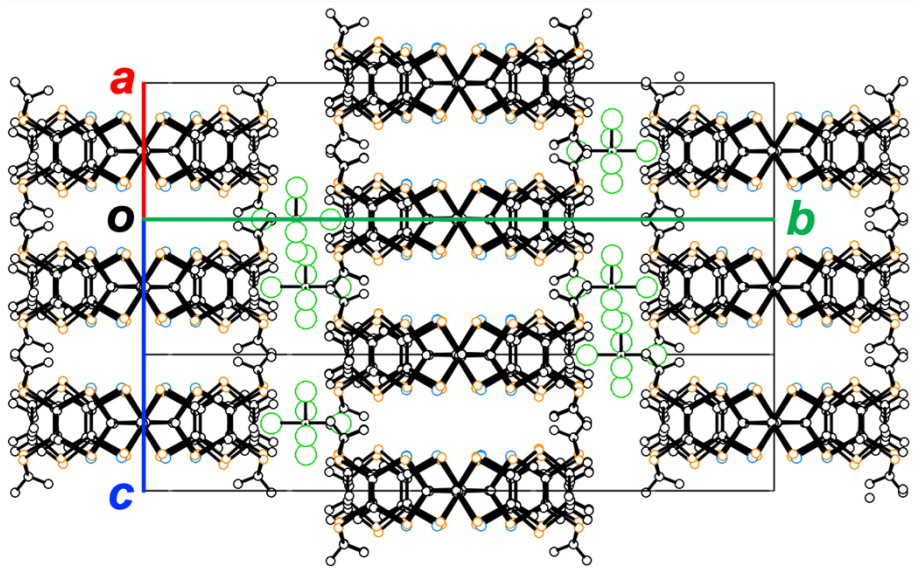

Figure S7. Crystal structures of (**1**)PF_6 viewed along the molecular stacking axis at 296 K.

Table S4. Selected anisotropic displacement parameters U_{ij} (i,j = 1–3) of (**1**)PF_6.

atom	T / K	U_{11}	U_{22}	U_{33}	U_{23}	U_{13}	U_{12}
S1	50	0.0706(9)	0.0209(5)	0.0374(7)	−0.0159(5)	0.0413(7)	−0.0268(6)
	100	0.0420(6)	0.0174(5)	0.0231(5)	−0.0042(4)	0.0181(5)	−0.0102(5)
	120	0.0453(4)	0.0219(3)	0.0272(3)	−0.0029(3)	0.0180(3)	−0.0088(3)
	296	0.1003(9)	0.0422(6)	0.0656(7)	−0.0032(5)	0.0415(7)	−0.0147(6)
S2	50	0.0571(8)	0.0310(6)	0.0303(6)	−0.0201(5)	0.0309(6)	−0.0276(6)
	100	0.0346(6)	0.0212(5)	0.0222(5)	−0.0081(4)	0.0142(5)	−0.0062(5)
	120	0.0409(4)	0.0252(3)	0.0268(3)	−0.0078(3)	0.0158(3)	−0.0040(3)
	296	0.0987(9)	0.0548(6)	0.0649(7)	−0.0206(5)	0.0402(7)	−0.0081(6)
C7	50	0.030(2)	0.017(2)	0.024(2)	−0.0087(17)	0.0145(19)	−0.0145(18)
	100	0.0193(19)	0.0104(17)	0.0179(19)	−0.0015(15)	0.0050(16)	−0.0036(15)
	120	0.0212(12)	0.0178(12)	0.0231(13)	−0.0026(9)	0.0066(10)	−0.0032(10)
	296	0.049(2)	0.0348(18)	0.047(2)	−0.0025(15)	0.0181(17)	−0.0060(15)
C8	50	0.027(2)	0.024(2)	0.022(2)	−0.0104(18)	0.0143(19)	−0.0166(19)
	100	0.0178(18)	0.0156(18)	0.0167(19)	−0.0035(15)	0.0055(16)	−0.0056(15)
	120	0.0234(13)	0.0199(12)	0.0205(12)	−0.0026(9)	0.0074(10)	−0.0043(10)
	296	0.048(2)	0.043(2)	0.046(2)	−0.0085(16)	0.0165(18)	−0.0066(17)
C9	50	0.0102(17)	0.027(2)	0.0100(18)	0.0022(16)	0.0010(15)	0.0015(16)
	100	0.0117(17)	0.0192(18)	0.0126(19)	0.0007(15)	0.0034(15)	0.0008(15)
	120	0.0171(11)	0.0217(12)	0.0167(11)	0.0000(9)	0.0047(9)	0.0012(10)
	296	0.0378(19)	0.0398(19)	0.0379(18)	0.0006(15)	0.0112(15)	0.0008(15)
C10	50	0.0119(17)	0.023(2)	0.016(2)	0.0083(16)	0.0047(15)	0.0030(16)
	100	0.0149(17)	0.0176(18)	0.0132(18)	0.0023(15)	0.0071(15)	0.0037(15)
	120	0.0157(11)	0.0225(12)	0.0201(12)	0.0025(9)	0.0051(9)	0.0018(10)
	296	0.0356(19)	0.042(2)	0.0445(19)	0.0058(15)	0.0122(16)	0.0034(15)

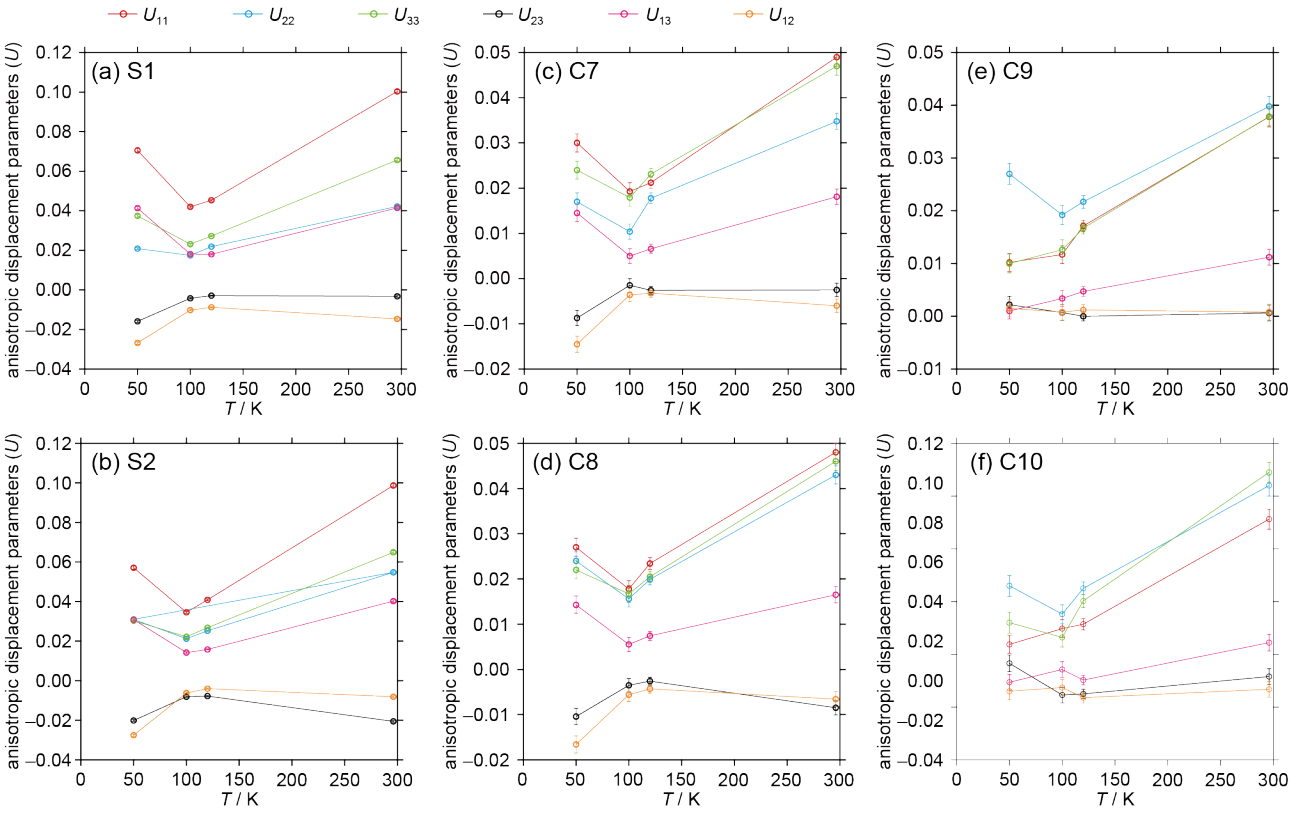

Figure S8. Temperature dependences of the anisotropic displacement parameters U_{ij} (i,j = 1—3) of (a) S1, (b) S2, (c) C7, (d) C8, (e) C9, and C10 atoms in (**1**)PF_6.

7. Theoretical calculations

The theoretical calculations of the triad (**1**) in (**1**)PF_6 were carried out based on density functional theory (DFT) using B3LYP/6-31G(d,p). DFT calculations were performed in the Gaussian 16 program package.[S7]

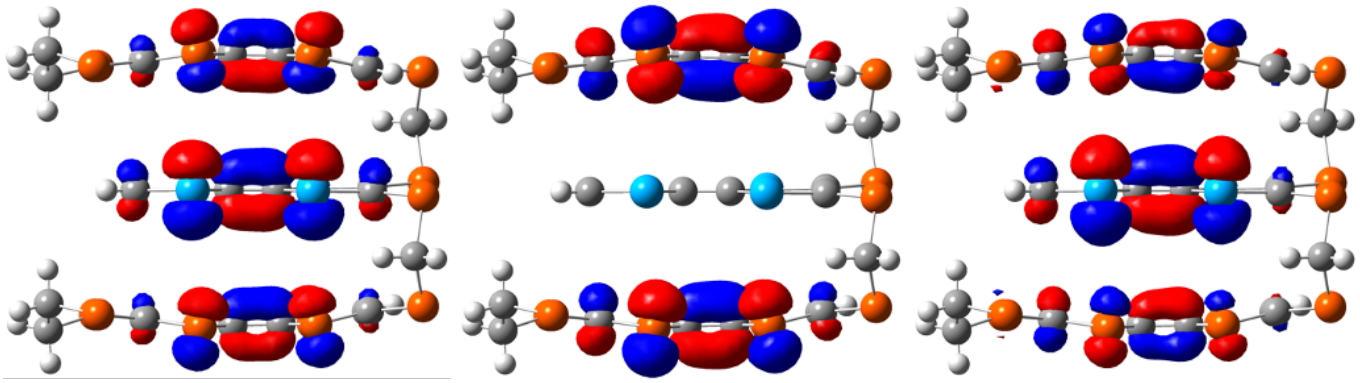

HOMO: –3.936 eV HOMO–1: –4.360 eV HOMO–2: –4.767 eV

Figure S9. HOMO, HOMO–1, and HOMO−2 (side views) of the triad**1** in (**1**)PF_6 at 296 K.

Table S5. The energy level of HOMO, HOMO–1, and HOMO−2 of the triad **1** in (**1**)PF_6 based on the DFT calculation.

T / K	296	120	100	50
HOMO / eV	–3.936	–3.919	–3.927	–3.926
HOMO–1 / eV	–4.360	–4.368	–4.368	–4.375
HOMO–2 / eV	–4.767	–4.796	–4.805	–4.809

8. Band calculation[S8]

Based on the X-ray structure analysis, the intermolecular overlap integrals (*S*) were calculated using the HOMOs of the triad (**1**) obtained by the extended Hückel MO calculations. Semiempirical parameters for the Slater-type atomic orbitals listed in Table S6 were used.[S9] We assumed the transfer integrals (*t*) to be proportional to the overlap integrals, $t = ES$ ($E = -10$ eV). The electronic band structures, density of states, and Fermi surfaces were calculated using intermolecular transfer integrals based on the tight-binding approximation.

Table S6. Semiempirical parameters for Slater-type atomic orbitals.

orbitals	ζ	I_p / Ryd
Se 3s	2.44	−1.471
Se 3p	2.07	−0.794
Se 3d	1.50	−0.400
S 3s	2.122	−1.47
S 3p	1.827	−0.808
S 3d	1.50	−0.40
C 2s	1.625	−1.573
C 2p	1.625	−0.838
H1s	1.00	−1.0

Table S7. Overlap integrals[a] ($\times 10^{-3}$) and geometrical parameters[b] in (**1**)PF_6.

296 K	S	ϕ / °	x / Å	y / Å	z / Å
$a1$	–27.3	89.7	0.01	0.02	3.68
$a2$	21.8	88.7	1.66	0.08	3.62
$c1$	–2.5	13.8	1.80	6.15	1.51
$c2$	5.0	18.7	0.13	6.23	2.11
p	7.2	19.5	1.62	6.13	2.17
q	10.5	12.3	1.40	6.25	1.36

120 K	S	ϕ / °	x / Å	y / Å	z / Å
$a1$	–29.3	89.9	0.02	0.01	3.64
$a2$	23.9	88.2	1.63	0.11	3.56
$c1$	–2.4	13.3	1.80	6.08	1.44
$c2$	5.5	18.9	0.17	6.19	2.12
p	7.4	19.8	1.65	6.09	2.20
q	10.8	12.5	1.40	6.16	1.36

100 K	S	ϕ / °	x / Å	y / Å	z / Å
$a1$	–29.4	89.9	0.02	0.01	3.63
$a2$	24.1	88.2	1.63	0.11	3.55
$c1$	–2.3	13.2	1.81	6.07	1.43
$c2$	5.3	19.0	0.18	6.18	2.13
p	7.6	19.9	1.66	6.08	2.20
q	11.0	12.3	1.39	6.16	1.34

50 K	S	ϕ / °	x / Å	y / Å	z / Å
$a1$	–29.7	89.8	0.04	0.01	3.62
$a2$	25.2	87.9	1.61	0.13	3.53
$c1$	–2.5	13.5	1.79	6.06	1.46
$c2$	5.9	18.6	0.18	6.19	2.08
p	7.5	19.6	1.64	6.07	2.16
q	11.3	12.5	1.37	6.14	1.37

a) Definition of intermolecular interactions $a1$, $a2$, $c1$, $c2$, p, and q are depicted in Figures 3c and S10.
b) See reference S10.

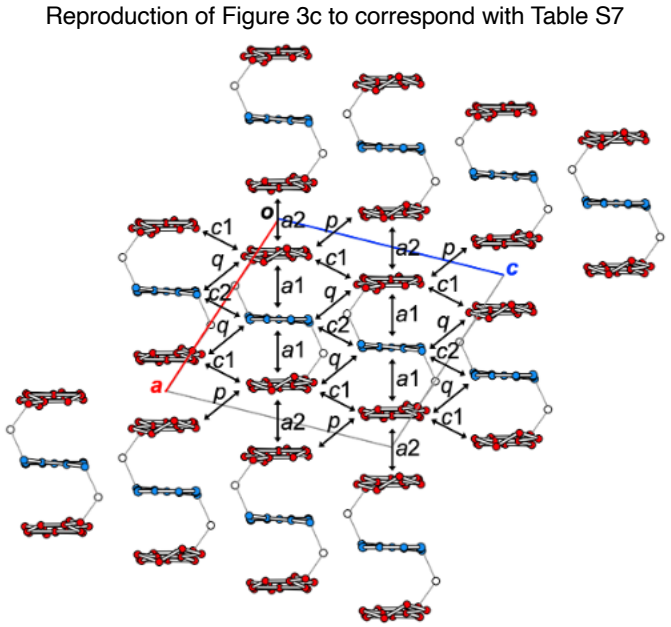

Figure S10. Conducting sheet of (**1**)PF_6 viewed along the donor long axis at 296 K.

Table S8. The HOMO energy of donor units in (**1**)PF_6 estimated from the extended Hückel MO calculation, assuming that the units were independent donor molecules from each other.

T / K	296	120	100	50
Unit A / eV	–9.334	–9.348	–9.346	–9.347
Unit B / eV	–9.488	–9.492	–9.496	–9.497

Table S9. Bandwidth (W_U W_M, and W_L)[a] and bandgap (Gap 1 and Gap 2)[a] in (**1**)PF_6.

T / K	296	120	100	50
W_U / eV	0.30	0.33	0.33	0.34
W_M / eV	0.43	0.48	0.49	0.50
W_L / eV	0.29	0.31	0.32	0.32
Gap 1 / eV	0.05	0.04	0.04	0.04
Gap 2 / eV	0.19	0.17	0.16	0.17

a) Definitions of W_U, W_M, W_L, Gap 1, and Gap 2 are depicted in Figures 4, S11, and S12.

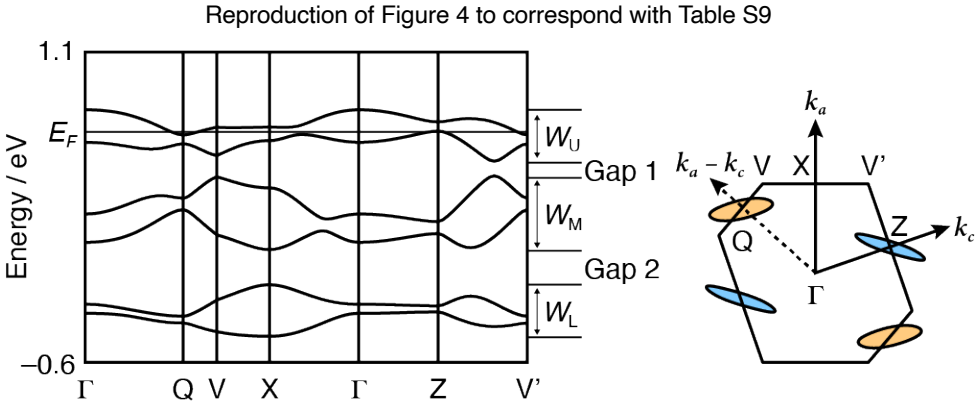

Figure S11. Calculated band dispersion and Fermi surfaces of (**1**)PF_6 at 296 K (Phase 1). Q = (0.5, 0, –0.5), X = (0.5, 0, 0), and Z = (0, 0, 0.5). Hole and electron pockets are represented in light blue and orange circles, respectively.

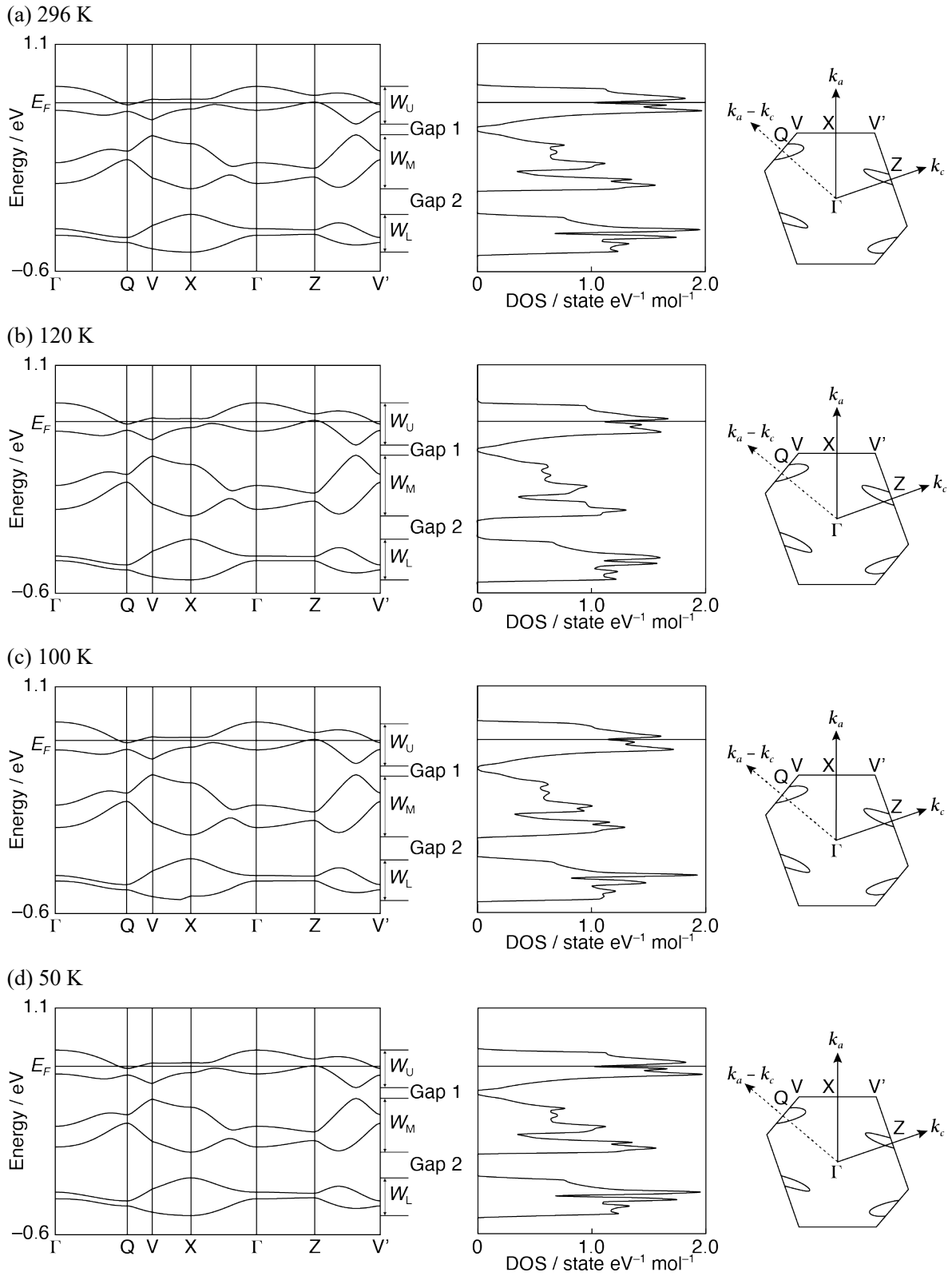

Figure S12. Calculated band dispersion, density of states (DOS) and Fermi surfaces of (**1**)PF_6 assuming that the units should be independent donor molecules from each other at (a) 296, (b) 120, (c) 100, and (d) 50 K. Q = (0.5, 0, –0.5), X = (0.5, 0, 0), and Z = (0, 0, 0.5).

9. NMR spectra data

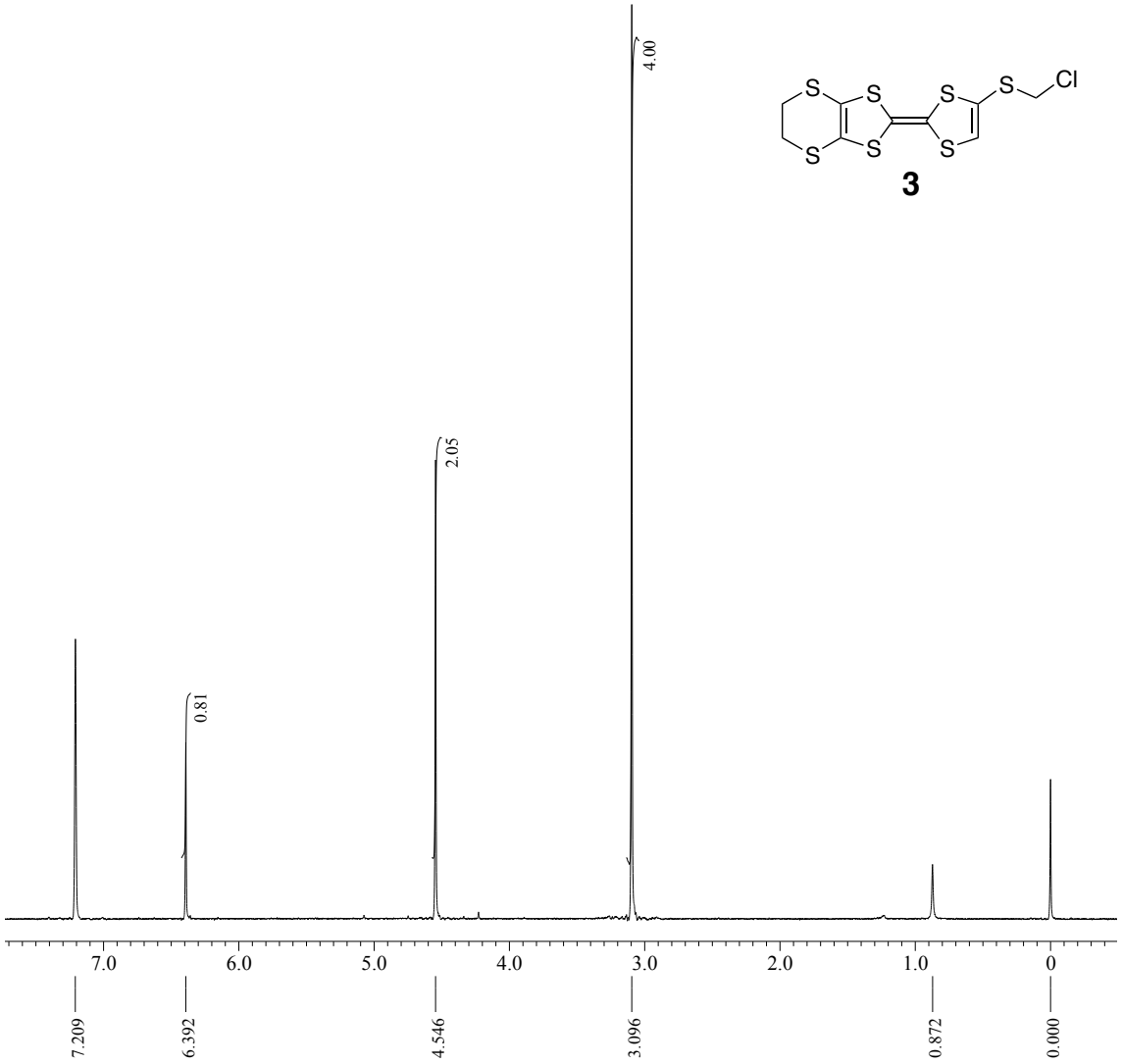

Figure S13. ^{1}H NMR spectrum of compound **3** in CS_2/C_6D_6.

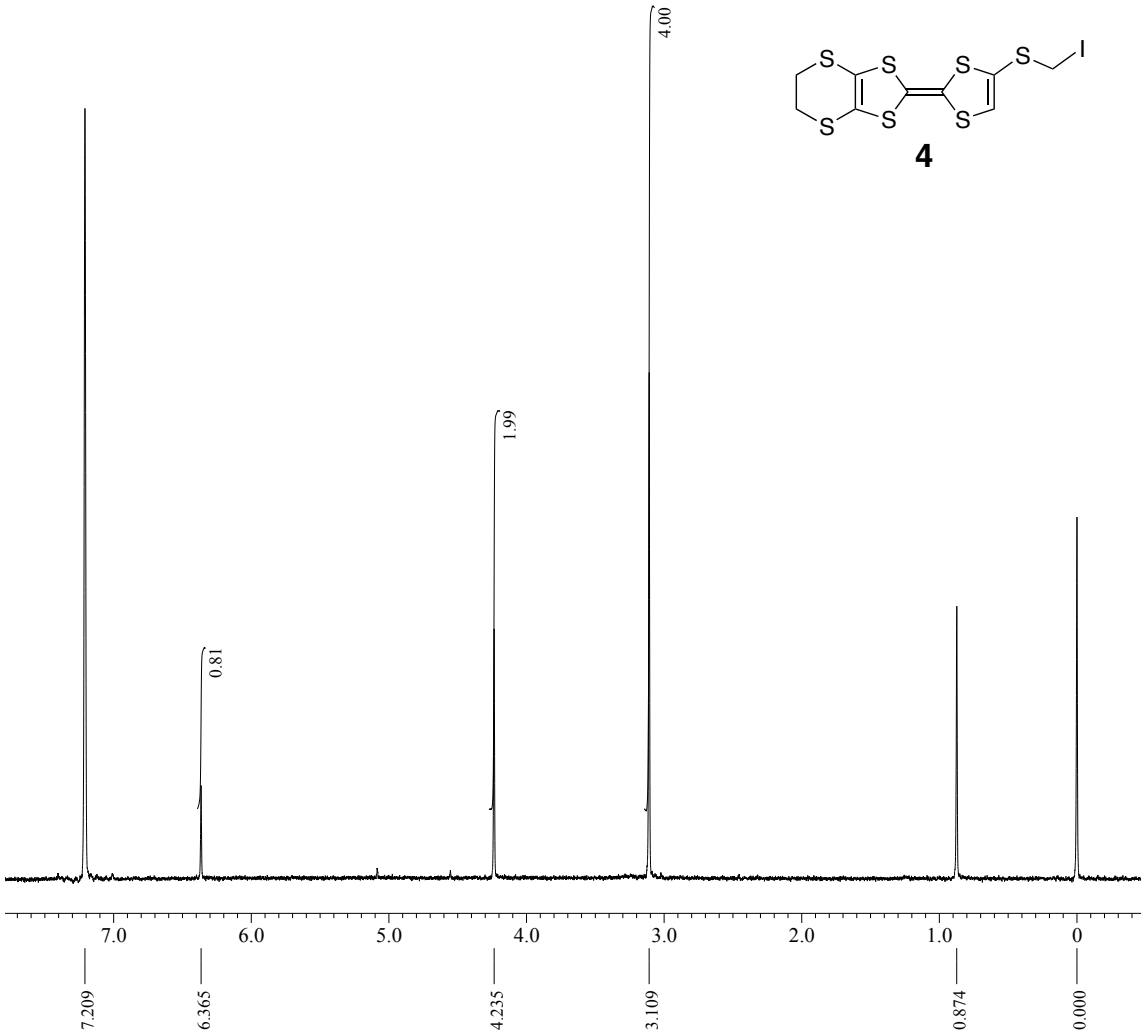

Figure S14. ^{1}H NMR spectrum of compound **4** in CS_2/C_6D_6.

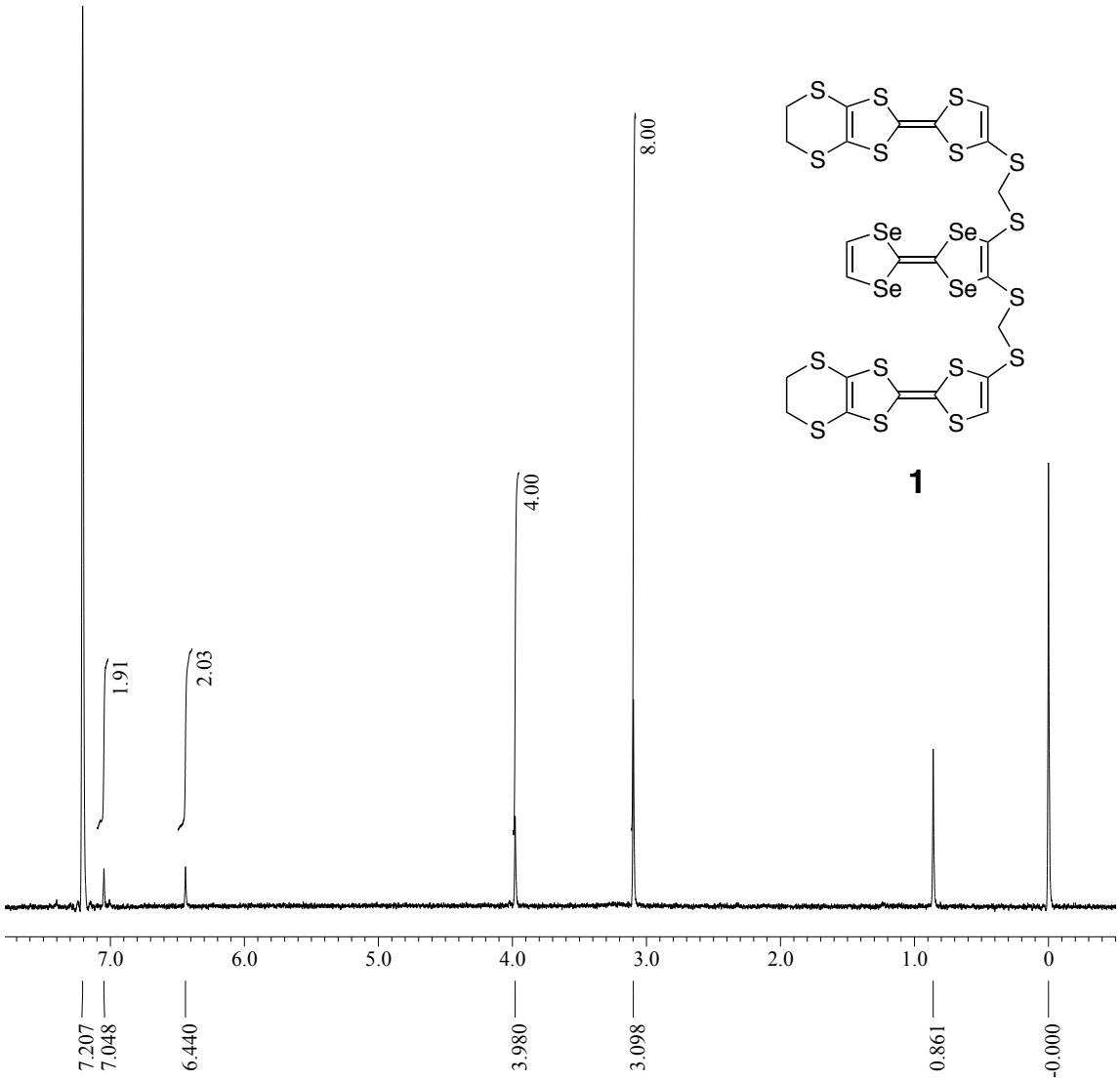

Figure S15. ^{1}H NMR spectrum of triad (**1**) in CS_2/C_6D_6.

References

S1. C. Jia, D. Zhang, X. Guo, S. Wan, W. Xu and D. Zhu, *Synthesis*, 2002, **2002**, 2177–2182.

S2. K. Takimiya, Y. Kataoka, N. Niihara, Y. Aso and T. Otsubo, *J. Org. Chem.*, 2003, **68**, 5217–5224.

S3. *CrysAlisPro (ver. 1.171.42.49)*: Data Collection and Processing Software, Rigaku Corporation (2015). Tokyo 196-8666, Japan.

S4. R. C. Clark and J. S. Reid, *Acta Crystallogr. A*, 1995, **51**, 887–897.

S5. *SHELXT*: G. M. Sheldrick, *Acta Crystallogr A Found Adv*, 2015, **71**, 3–8.

S6. *SHELXL*: G. M. Sheldrick, *Acta Crystallogr. C*, 2015, **71**, 3–8.

S7. Gaussian 16, Revision C.01, M. J. Frisch, G. W. Trucks, H. B. Schlegel, G. E. Scuseria, M. A. Robb, J. R. Cheeseman, G. Scalmani, V. Barone, G. A. Petersson, H. Nakatsuji, X. Li, M. Caricato, A. V. Marenich, J. Bloino, B. G. Janesko, R. Gomperts, B. Mennucci, H. P. Hratchian, J. V. Ortiz, A. F. Izmaylov, J. L. Sonnenberg, D. Williams-Young, F. Ding, F. Lipparini, F. Egidi, J. Goings, B. Peng, A. Petrone, T. Henderson, D. Ranasinghe, V. G. Zakrzewski, J. Gao, N. Rega, G. Zheng, W. Liang, M. Hada, M. Ehara, K. Toyota, R. Fukuda, J. Hasegawa, M. Ishida, T. Nakajima, Y. Honda, O. Kitao, H. Nakai, T. Vreven, K. Throssell, J. A. Montgomery, Jr., J. E. Peralta, F. Ogliaro, M. J. Bearpark, J. J. Heyd, E. N. Brothers, K. N. Kudin, V. N. Staroverov, T. A. Keith, R. Kobayashi, J. Normand, K. Raghavachari, A. P. Rendell, J. C. Burant, S. S. Iyengar, J. Tomasi, M. Cossi, J. M. Millam, M. Klene, C. Adamo, R. Cammi, J. W. Ochterski, R. L. Martin, K. Morokuma, O. Farkas, J. B. Foresman, D. J. Fox, Gaussian, Inc. (2016). Wallingford CT, USA.

S8. T. Mori, A. Kobayashi, Y. Sasaki, H. Kobayashi, G. Saito and H. Inokuchi, *Bull. Chem. Soc. Jpn.*, 1984, **57**, 627–633.

S9. T. Mori and M. Katsuhara, *J. Phys. Soc. Jpn.*, 2002, **71**, 826–844.

S10. T. Mori, *Bull. Chem. Soc. Jpn.*, 1998, **71**, 2509–2526.